Journal of Structural Geology, Vol. 9, No. 4, pp. 457 to 472, 1987
Printed in Great Britain

0191-8141/87 $03.00 + 0.00

Relationships of rock cleavage fabrics to incremental and accumulated strain in the Conococheague Formation, U.S.A.

BRYAN TAPP

Department of Geosciences, The University of Tulsa, Tulsa, OK 74104, U.S.A.

and

JOHN WICKHAM *

School of Geology and Geophysics, The University of Oklahoma, Norman, OK 73019, U.S.A.

(*Received* 25 *February* 1986; *accepted in revised form* 3 *November* 1986)

Abstract—Pressure solution coupled with twin gliding, and recrystallization acted to form two geometrically distinct cleavages in the Conococheague Formation, northwest Virginia and West Virginia. Limestone layers contain a penetrative cleavage (S_p) formed by pervasive pressure solution (Coble creep), with twin gliding in more highly deformed zones. Dolomite layers contain a spaced solution cleavage (S_s) formed by pressure solution, also with twin gliding in highly deformed zones. Recrystallization textures occur in highly deformed zones of limestones and dolomites. Incremental strain shows that layering was initially inclined as much as 30° to shortening, and that the deformation was locally non-coaxial, as viewed by the deforming material on the fold limbs. Spaced cleavage zones are curved, and closely match the initial and final orientations of incremental elongation. Penetrative cleavage parallels the elongation axis of accumulated strain (measured using deformed ooids). Pressure solution surfaces in dolomites concentrate insoluble materials. Deformation, together with twin gliding, and recrystallization are greatest in the hinge zones of folds and least on shallowly dipping limbs of asymmetric folds. The deformation mechanism path of calcite and dolomite are similar; changing from pressure solution to twin gliding with recrystallization as strain rate (strain energy density) increases.

INTRODUCTION

THE PURPOSE of this report is to: (1) describe the relationship between strain history and cleavage fabrics and textures in naturally deformed limestones and dolomites; (2) to determine which deformation mechanism(s) acted to form the cleavage fabrics and textures observed; and (3) to determine the relative timing of the mechanisms where the deformation is non-coaxial.

This study concentrates on rock cleavage in the Cambrian Conococheague Formation in northwestern Virginia, and a portion of the West Virginia Panhandle (Fig. 1). The Conococheague Formation was chosen for two reasons. (i) It contains both incremental and accumulated strain markers in the form of calcite fibers and ooids. (ii) There are two distinct lithologies, limestone and dolomite, with two distinct cleavage types: penetrative cleavage (termed S_p) characterized by morphologic alignment of rock constituents (Cloos 1947, 1971); and a spaced cleavage (termed S_s) characterized by sinuous zones of phyllosilicates, largely clays (Wickham 1972). The penetrative cleavage has been described as a slaty cleavage (Wickham 1972, Edmundson & Nunan 1973), or simply as cleavage (Cloos 1971). The spaced cleavage has been described as a fracture cleavage (Edmundson & Nunan 1973) following the convention of De Sitter (1964), and as a solution cleavage (Wickham 1972). The terms S_p and S_s used in this paper do not carry any relative timing or genetic connotations.

The study area is just south of the location of the classical work by Cloos (1947) and is in the northern part of his later work (Cloos 1971). The local deformation can be approximated by plane strain on surfaces normal to the fold hinge line (Cloos 1971). Folding and cleavage preserved in the area are from a single, progressive event (Wickham 1972) resulting in a uniform deformation style in the study area (Cloos 1947, 1971). Folds in the study area are asymmetric, with overturned northwest limbs, and the hinge surfaces dip SE (Wickham 1972, Wickham & Anthony 1978). The deformation path is locally non-coaxial (Wickham 1973, Wickham & Anthony 1978). The Conococheague, therefore, represents a unique opportunity to examine the formation of rock cleavage in more than one lithology, and in a system where deformation intensity and history can be determined.

Conditions of deformation

Overburden and temperature conditions during deformation of the Conococheague can be estimated. Although chlorite is present in some cleavage zones, it can form over such a wide range of temperatures that it is of little use as a temperature indicator.

The initial temperature of deformation can be estimated from the overburden based on reported sediment thicknesses, and a normal continental geothermal gra-

* Present address: Mobil Research Lab, P.O. Box 819047, Dallas, TX 75381-9047, U.S.A.

dient. If the study area had been covered by sediments up to and including the Mississippian clastic sequence, the overburden thickness would have been about 6.6 km (Butts 1973). A geothermal gradient of 15°C/km would yield a temperature of 120°C, and 25°C/km about 180°C. Patalakha & Polyakov (1977) showed that at the effective viscosity of the rock units in question (10^{22}–10^{24} Poises) the maximum contribution of viscous heating over 10 million years would be approximately 12°C. Deformation of the Conococheague Formation probably initiated in catagenic to metagenic conditions between 120–180°C, and never exceeded lower epimetamorphic conditions.

SUMMARY OF CLEAVAGE FORMATION MECHANISMS

Rock cleavage has been studied for over a century and there has been great progress in understanding its nature and origin. However, there is not agreement on a classification for rock cleavage (see Borradaile *et al.* 1982). Rock cleavage is found in a wide variety of lithologies, ranging from moderately deformed sandstones, shales and carbonates to highly deformed metamorphic rocks and meta-igneous rocks (Siddans 1972; Wood 1974). Cleavage forms in a variety of deformation environments, can be delineated by a variety of rock textures, and may form in response to more than one deformation mechanism (e.g. Groshong *et al.* 1984). The mechanisms of rock deformation are dependent on deviatoric stress, strain rate, strain energy density, strain path, temperature, crystal size and composition (Freeman & Ferguson 1986). A reproducible relation between the formation of rock fabrics, and the conditions and history of deformation in naturally deformed rocks has not yet been formulated (Freeman & Ferguson 1986).

The formation of cleavage can be treated as a physical process, a chemical process, or as a combination of both. Physical processes can be divided into intercrystalline mechanisms (physical rotation and translation), and intracrystalline mechanisms (twin and translation glide or slip). Chemical mechanisms include intercrystalline mechanisms (pressure solution), and intracrystalline mechanisms (thermally induced recrystallization and neomorphism).

Physical processes

Rotation. Cleavage in slates forms, in part, by the rotational alignment of platy particles, primarily phyllosilicates, from a random or nearly random orientation, as suggested by Sorby (1853), and verified by Tullis (1976) and Willis (1977) using the Jeffery (1923) and March (1932) models. Formation of slaty cleavage has been attributed to rotation of platy particles in unlithified sediment during dewatering based on the similarity of sedimentary dike orientations to cleavage orientation (Maxwell 1962; Alterman 1973; Clark 1974; Powell 1974; Roy 1978). Many others have concluded that slaty cleavage forms in lithified sedimentary rocks during deformation, and that the near parallelism of cleavage and clastic dikes is the result of strain (Epstein & Epstein 1969; Boulter 1974; Wood 1974; Geiser 1974, 1975; Holeywell & Tullis 1975; Beutner 1978, 1980). Although the formation of fabrics in unlithified sediments does occur (Williams *et al.* 1969; Means 1977), the truncation and deformation of rock constituents, and the formation of cleavage in a variety of rock types, is best explained by formation of cleavage after lithification (Wood 1974). Dewatering and physical rotation have never been suggested as major deformation mechanisms in the carbonate rocks of this area.

Ductile flattening. During deformation rock grains may form a morphologic, and/or a crystallographic preferred orientation, by plastic flattening and elongation [twin and translation gliding or slip, see Langdon (1985) for a review of ductile deformation]. Quartz, olivine and the carbonate minerals, aragonite, calcite and dolomite, have been studied extensively, and their deformation in controlled conditions is reasonably well understood (see Price 1985; Mercier 1985; Wenk 1985, respectively).

Strong preferred orientation fabrics can develop in cold working of limestones and dolomites (below 400°C) by intracrystalline (plastic) deformation (Wenk *et al.* 1973; Wagner *et al.* 1982; Wenk *et al.* 1986). Experimental studies using fine-grained limestones produce marked dimensional elongation at strains in the range 15–22%, but dimensional elongation does not appreciably increase after 22% shortening (Wagner *et al.* 1982). The dimensional elongation is accompanied by alignment of crystallographic planes in calcite [see Wagner *et al.* (1982) for a complete discussion]. In experimental studies dolomite does not produce strongly oriented crystallographic fabrics below 700°C (Wenk & Shore 1975).

Rutter (1974) estimated that at geologic strain rates below 400°C, limestones deform by twinning, slip and pressure solution; above 400°C, limestones deform by translation glide and twinning glide. Rutter & Rusbridge (1977) found that hot working in non-coaxial deformation produces morphologic elongation of calcite statistically perpendicular to the axis of maximum finite shortening and crystallographic orientations statistically perpendicular to the axis of maximum shortening of the last increment of deformation.

In naturally deformed limestones and dolomites, there is agreement that both the calcite and dolomite *c* axes (Bravais index {0001}) cluster around the normal to the foliation (Wenk & Shore 1975; Wenk *et al.* 1981), and that the calcite *a* axis (Bravais index $\{11\bar{2}0\}$) should lie along the foliation (Wenk *et al.* 1981). The formation of fabrics in progressive, non-coaxial, deformations can result in complex morphologic and crystallographic fabrics (Rutter & Rusbridge 1977, Dietrich & Song 1984).

Chemical mechanisms

Pressure solution. Pressure solution is the mass transfer of material from points of high stress to zones of

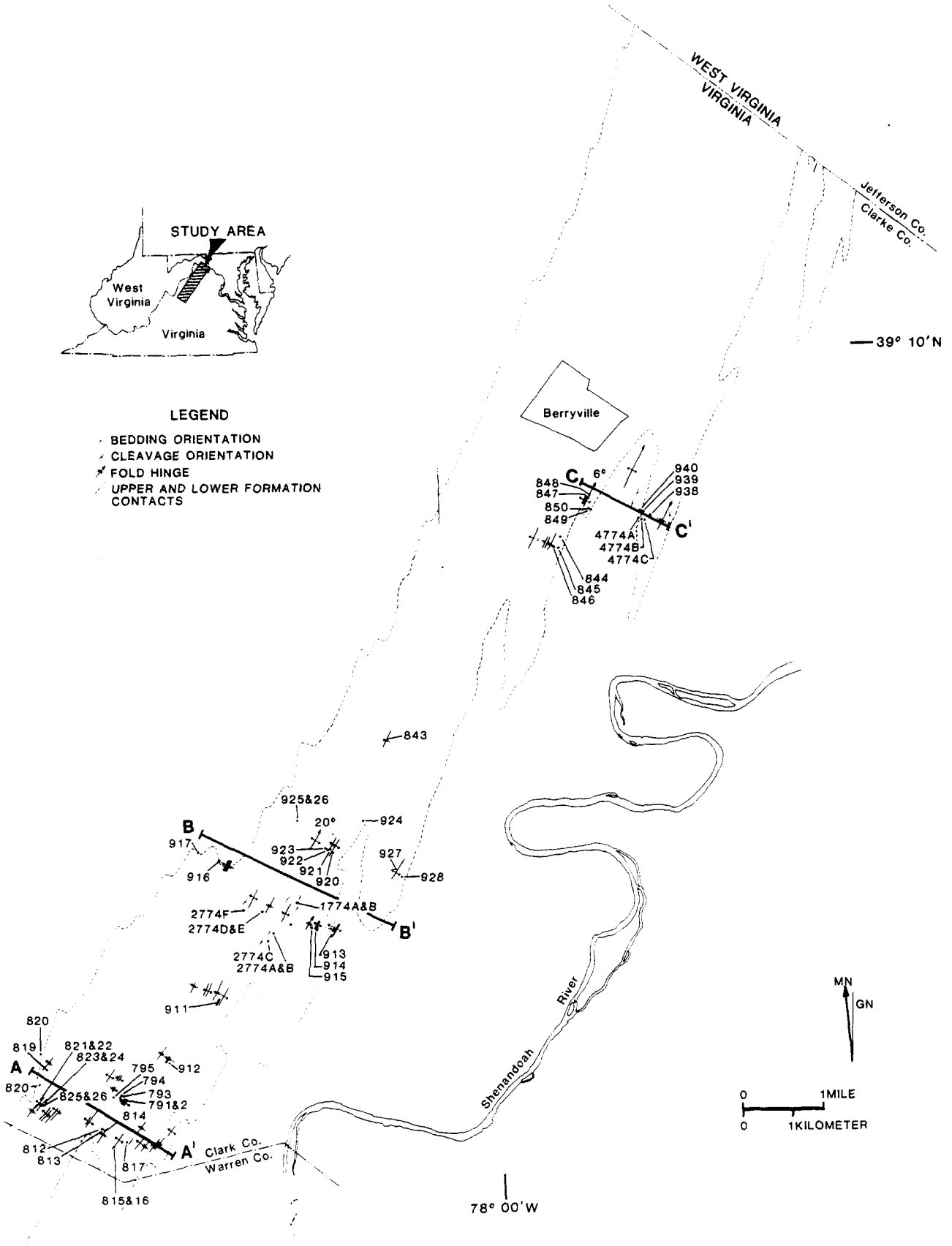

Fig. 1. Generalized map of study area showing locations of data points and traverses.

lower stress, in the presence of a fluid (Heald 1955; Weyl 1959; Ramsay 1967; Durney 1972, 1976; Groshong 1975a, De Boer 1977; Sprunt & Nur 1977; Fletcher & Pollard 1981; Fletcher 1982). Solution surfaces have been recognized as discrete cleavage surfaces by the truncation of fossils and rock particles, and by the presence of accumulated insoluble material on the solution cleavage surfaces (Plessman 1964, 1966). Pressure solution surfaces form normal to the direction of maximum principal stress (Weyl 1959; Durney 1972, 1976, 1978; Elliott 1973; Rutter 1976; De Boer 1977).

Pressure solution has been studied quantitatively and experimentally by Durney (1976) and Rutter (1976), who concluded that pressure solution is kinetically rapid enough to produce geologically realistic strain rates at low temperatures, and at low values of deviatoric stress.

Pressure solution has been documented as important in the formation of cleavage in slates, carbonates and sandstones (Durney 1972; Wickham 1972, Geiser 1974; 1975, Groshong 1975a,b, 1976; Gray 1978, 1981; Alvarez *et al.* 1978; Marshak & Engelder 1984), and as a pervasive phenomenon (Elliott 1973). The formation of discrete planar discontinuities is important in the interpretation of curved solution surfaces in folds (Groshong 1975b; Fletcher & Pollard 1981), and may indicate that solution surfaces initiate at a point and propagate outward as predicted by Fletcher & Pollard (1981).

Neomorphism and recrystallization. Neomorphism is the formation of new mineral phases during metamorphism or diagenesis (Spry 1968). Neomorphism in a deforming system results from the destruction of unstable phases, coupled with diffusion and growth of new, stable mineral constituents. The new lattice system will form with an orientation that is thermodynamically favorable with the stress field in which it forms (Kamb 1959).

Recrystallization is the thermally activated reorganization of a deformed crystal lattice lowering its free energy. The stages of recrystallization are recognizable by the associated morphologic signature (Hobbs *et al.* 1976). The lowest temperature stage is recovery, the removal of deformation induced dislocations by subgrain growth. New grain boundaries form within a strained crystal and sweep out dislocations, forming strain-free subgrains. Primary recrystallization forms high-angle crystal boundaries by continued migration of the boundaries. At higher temperatures, nearly equant minerals form to minimize the surface area to volume ratio. In highest grade metamorphism, large crystals form at the expense of smaller crystals, as crystal boundaries sweep through the material during secondary recrystallization. In low grade metamorphic rocks recrystallization produces unstrained crystal lattices with high-angle crystal boundaries, and a preferred morphologic and crystallographic orientation (Wenk *et al.* 1973; Rutter 1974; Wenk & Shore 1975; Tullis 1976; Rutter & Rusbridge 1977). Recrystallization may occur after deformation (annealing) or as a syntectonic process.

FIELD OBSERVATIONS

Field area

Seven traverses across the Conococheague Formation were mapped on aerial photographs, and topographic maps (see Fig. 1). Fold hinge traces and orientations, and bedding and cleavage orientations were noted at each outcrop on the traverses. Oriented samples representing all cleavage types and occurrence were also collected for strain and fabric analysis. Idealized cross-sections were prepared by projection of the traverse data onto a fold profile plane, which was used to locate samples for comparison of accumulated and incremental strain histories across individual folds to cleavage geometry (Fig. 2). Additional fold hinge orientations were determined using statistical analysis on the sphere from bedding orientation data (after Watson 1970).

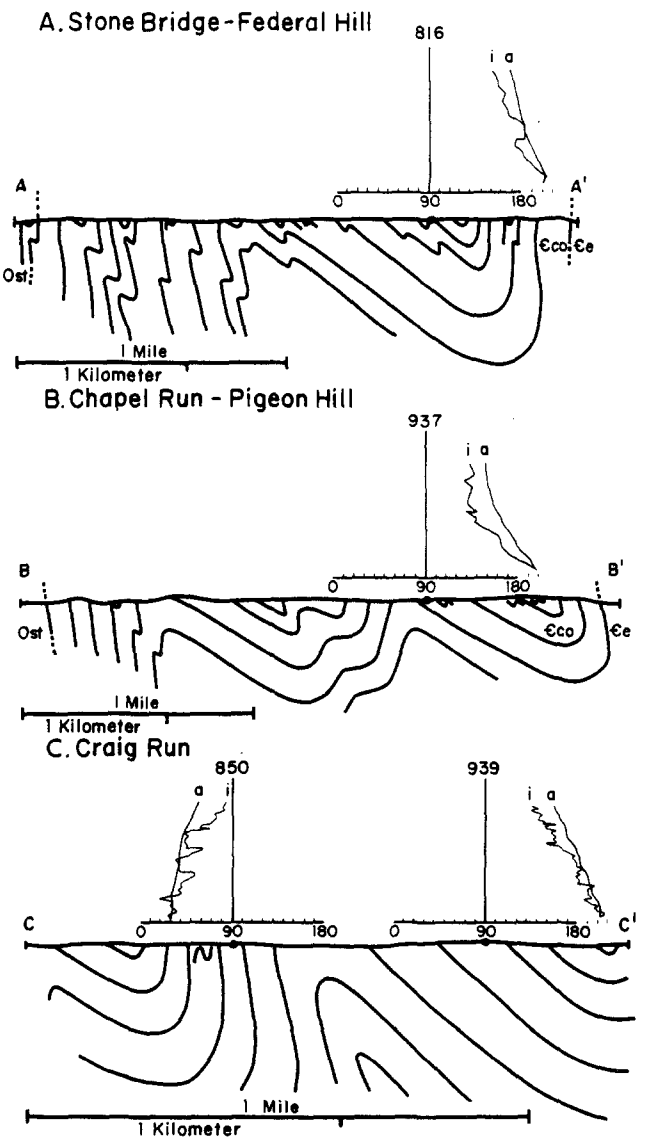

Fig. 2. Cross-sections showing composite incremental strain paths. Plots show orientation of incremental (i) and accumulated (a) elongation axis through time relative to bedding. The horizontal axis represents angle to bedding of the principal strain elongation axis. The vertical axis represents time.

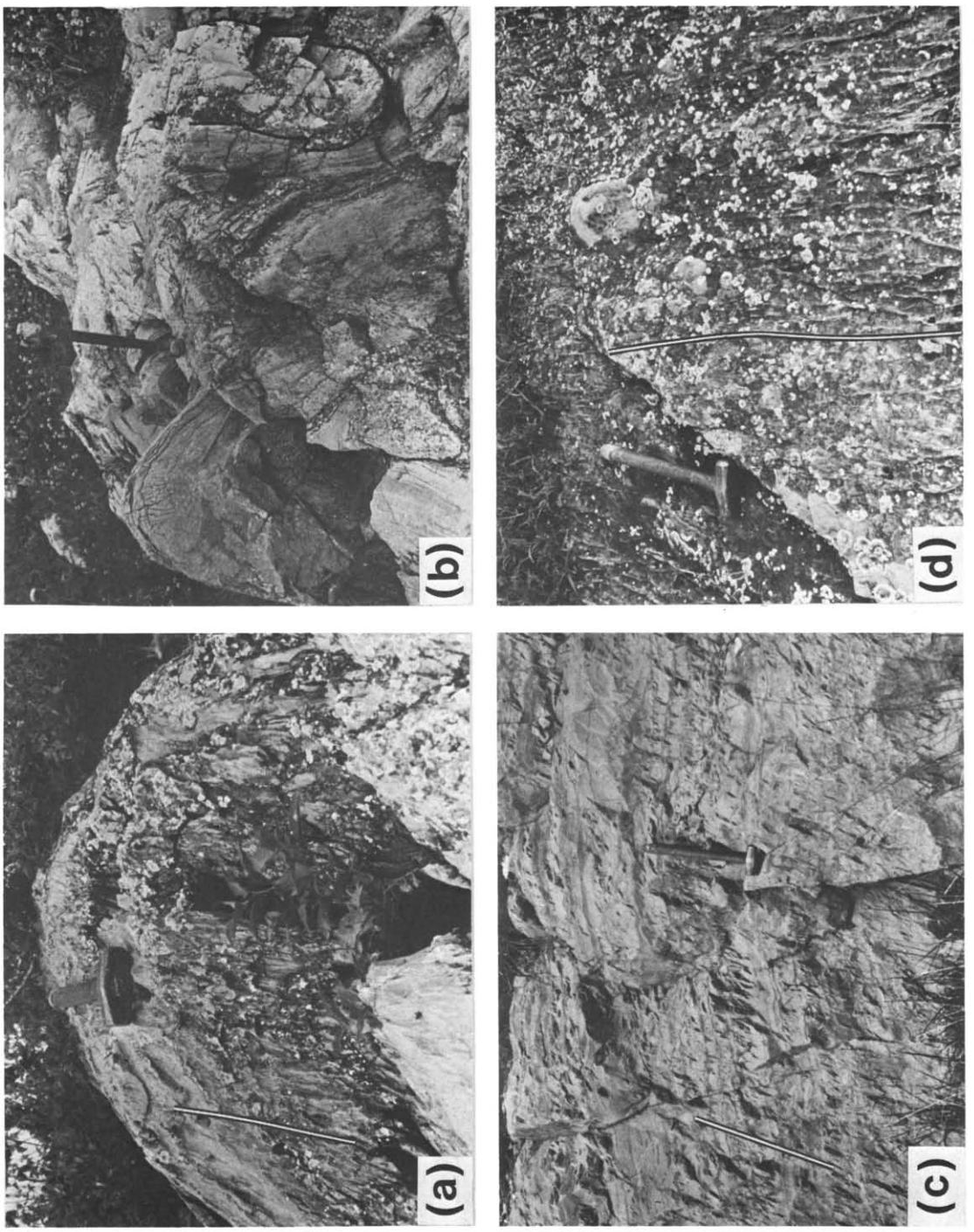

Fig. 3(a). Fold in ribbon rock facies of Conococheague, white on black line shows cleavage orientation. Head of hammer is 10 cm long. (b) Folds in units with thick dolomites. Compare the tightness of the folds in (a). Hammer handle is 35.6 cm long. (c) Outcrop showing character of cleavage. The outcrop is in the ribbon rock facies of the Conococheague, the darker horizontal bands are dolomite. Cleavage orientation is shown by the white on black line. The hammer handle is 35.6 cm long. (d) Bedding plane in dolomite showing sinuous character of spaced cleavage. The bedding plane is in the hinge zone of a minor syncline; view is downplunge. The head of the hammer is 10 cm long.

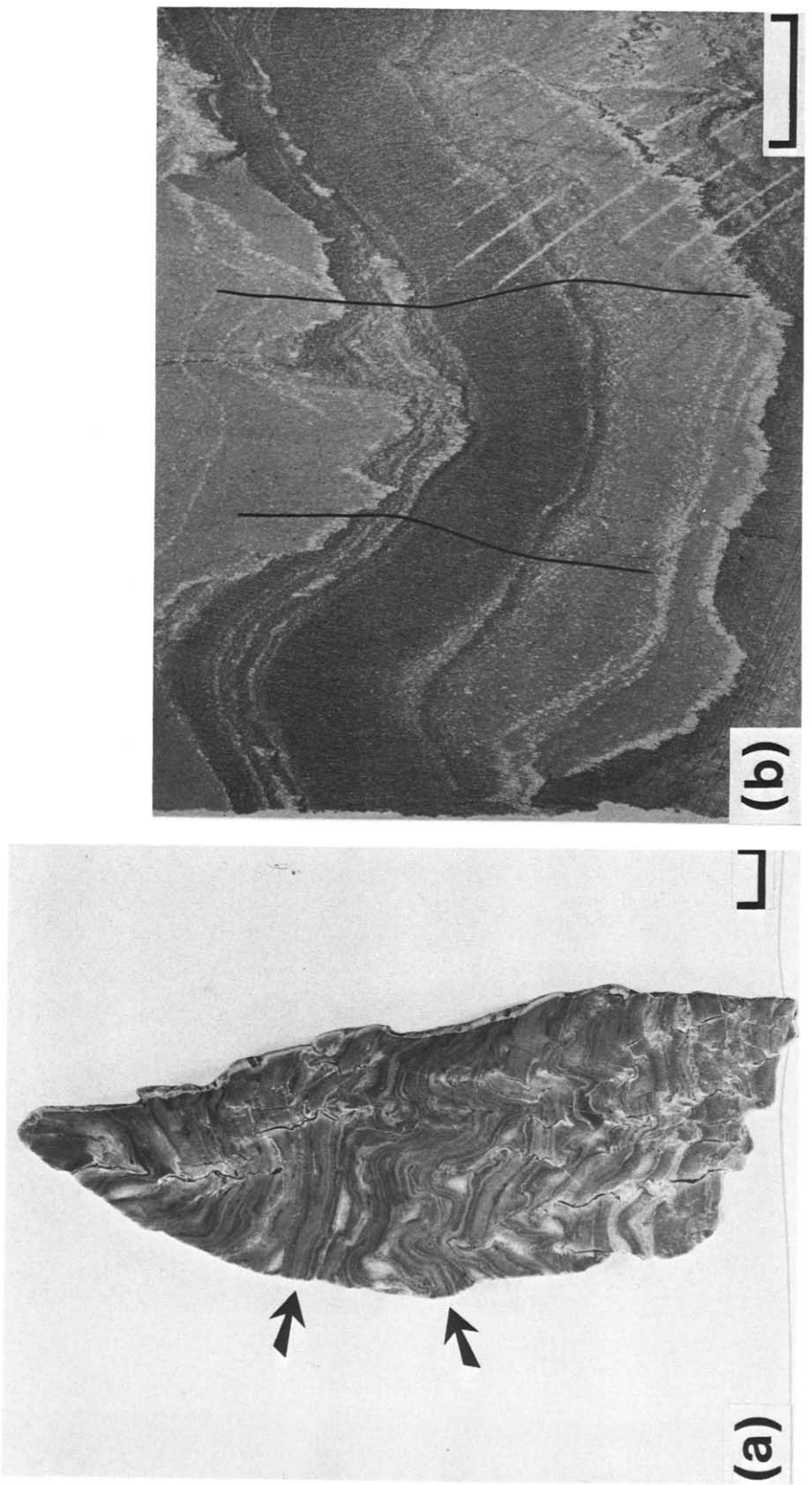

Fig. 4. (a) Polished slab from the hinge of a syncline. Note the difference in arclength of bedding from the dolomite (upper arrow) to the limestone layers (lower arrow). Scale bar is 2 cm. (b) Plane polarized photograph of thin section from hinge of minor syncline showing cleavage refraction at bedding contacts. Scale bar is 1 cm.

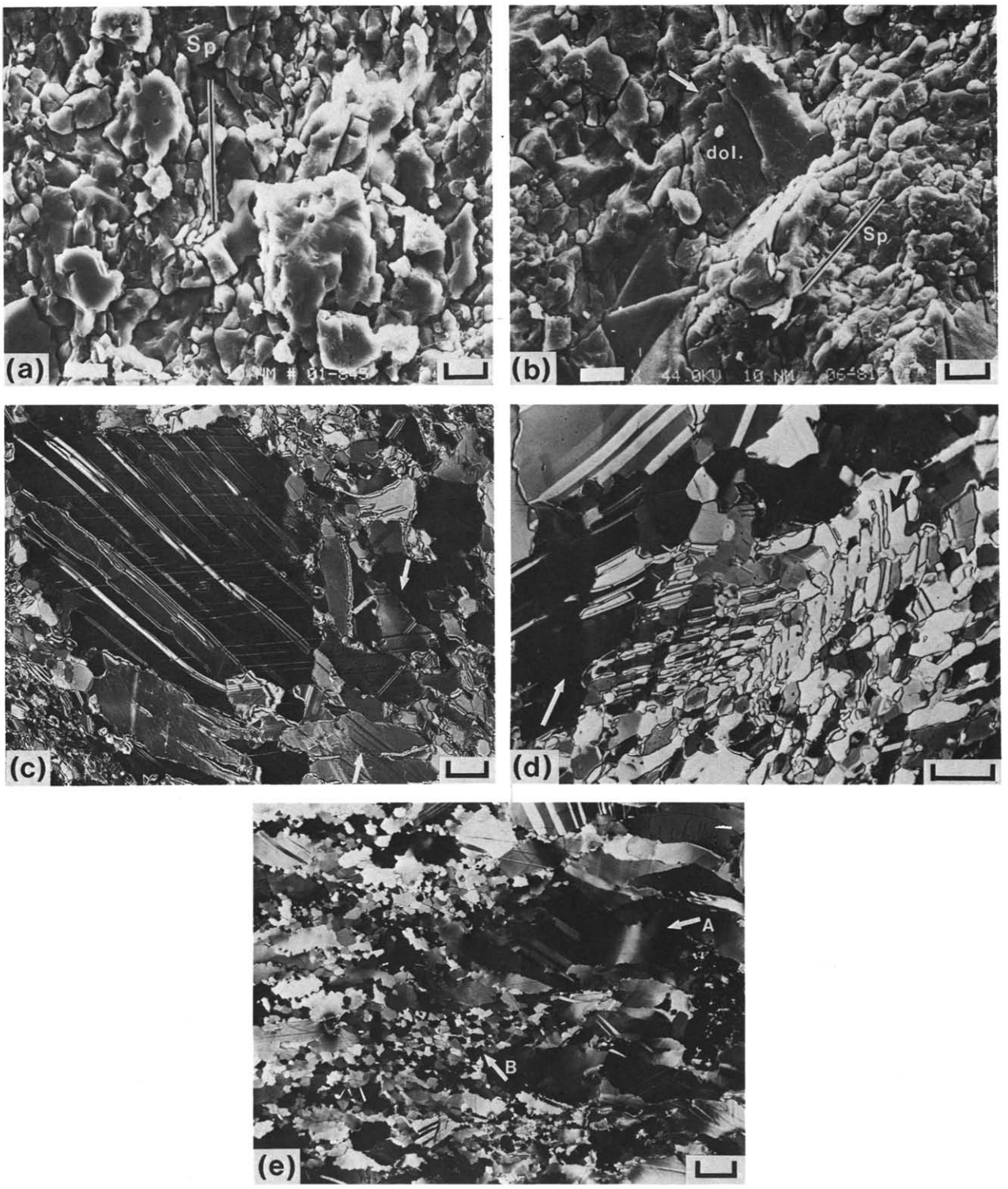

Fig. 5.(a). Scanning electron photomicrograph of penetrative cleavage (S_p) in sample 845. Penetrative cleavage is nearly vertical in the photograph, it is marked with a black on white line labelled S_p. The grains standing in relief are dolomite. The micrite has straight boundaries and some high angle boundaries. Scale bar is 18 microns long. (b) Serrated boundary of dolomite grain (top of dolomite grain, labelled dol., see white on black arrow) and concentration of phyllosilicates (bottom of same grain). The serrated boundary is interpreted as indicating pressure solution activity at the crystal boundary. Accumulated phyllosilicates show concentration of insoluble materials due to pressure solution. Penetrative cleavage is marked by a black and white line and is labelled S_p. Scale bar is 20 microns. (c) Photomicrograph of ultrathin section under crossed nicols showing subgrain growth of deformed calcite spar between white arrows. The fine twins in the spar, and other grains may be an artifact of section preparation. However, twinning is noted in many thin sections, regardless of the degree of thinning and polishing. Scale bar is 70 microns. (d) Crossed nicol photomicrograph of recrystallization of twinned calcite. Chevron subgrains (black arrow in upper right) are formed along old twins. New subgrains are growing at edge of crystal (white arrow, lower left) yielding texture similar to (c). Scale bar is 50 microns. (e) Crossed nicol photomicrograph of recrystallized vein fill in hinge of syncline. The calcite shows undulatory extinction (arrow A) and formation of subgrains (arrow B). Grain boundaries are bulbous, which may indicate grain boundary migration. Scale is 100 microns.

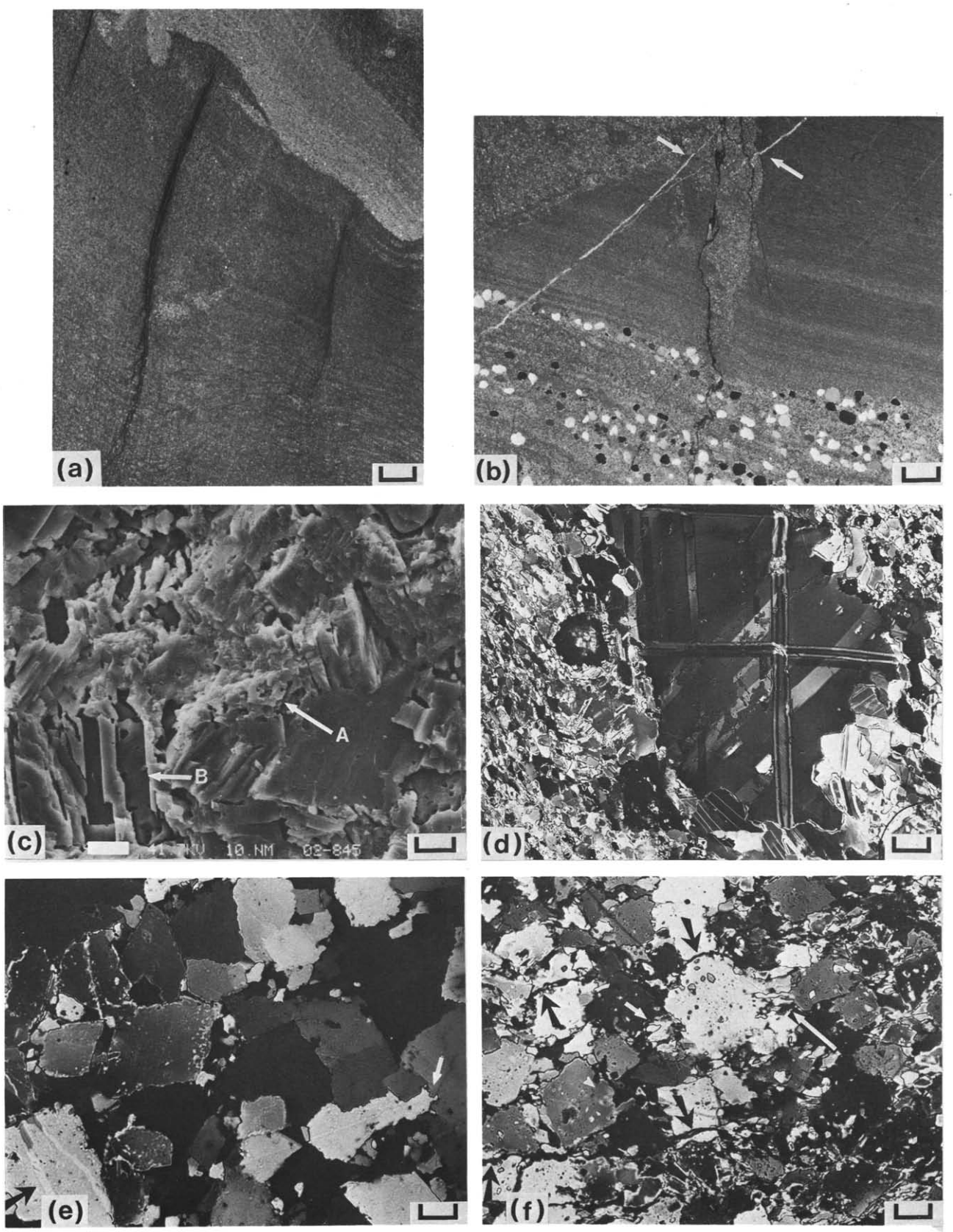

Fig. 6(a). Plane light photograph of a thin section showing curved, spaced cleavage near the hinge zone of a syncline. Scale is 2 mm. (b) Plane light photograph of a thin section from the shallow limb of a fold showing sinuous solution cleavage. Note the offset of the healed fracture (between arrows). Scale is 2 mm. (c) Scanning electron photomicrograph of apparent dolomite subgrain (arrow A) in a twinned dolomite field (arrow B). The sample is from the hinge of a minor fold; scale is 25 microns. (d) Crossed nicol photomicrograph of twinned dolomite in micrite. Note the replacement of the dolomite by calcite at the edges and the straight crystal boundaries of the calcite crystals. Scale is 70 microns. (e) Crossed nicol photograph of dolomite from the hinge of a minor fold. The sample shows twinning of the dolomite (black arrow, lower left) and apparent grain boundary migration (white arrow, right side), along with subgrain growth. Scale is 60 microns. (f) Crossed nicol photograph of dolomite from hinge of major fold showing small pressure solution surfaces (between black arrows; one in upper $\frac{1}{3}$ of photo, the other in the lower $\frac{1}{4}$ of the photo), and subgrain growth and possible grain boundary migration (white on black arrow in right $\frac{1}{3}$ of photo). Scale is 60 microns.

The Conococheague Formation

The Cambrian Conococheague Formation can be divided into three members. The lowermost unit is a sandy limestone containing ooids, rip-up clasts, algal mats and intercalated dolomite stringers. The middle member of the formation consists of regularly interbedded limestone and dolomite layers with thickness of the layers varying from 1 cm to 2 m. The upper member consists of thinly interbedded algal dolomites and limestones (termed ribbon-rock), and sandy bioclastic limestones. Crinoid and trilobite fragments are found in bioclastic layers.

Folds

Folds in the study area are generally asymmetric, type 1c (Ramsay 1967) folds that plunge gently to the northeast, averaging 6° at N30°E (Fig. 3a). The dip of the fold hinge surface does not vary systematically, and ranges from 60 to 84° SE. Fold asymmetry and tightness generally decrease from south to north, away from the nose of the Massanutten Synclinorium. Fold interlimb angle also depends on lithology; tighter folds are present in interlayered limestones and dolomites (Figs. 3a & b) where interlimb angles vary from 40 to 71°. Interlimb angles in dolostones are higher, varying from 85 to 90°.

Cleavage: general observations

Two distinct cleavage fabrics are present in the study area; a penetrative cleavage (S_p) and a spaced cleavage (S_s). In the field penetrative cleavage is expressed as a preferred direction of rupture and weathering, as well as alignment of rock constituents (Fig. 3c).

The spaced cleavage (S_s), consisting of regularly spaced clay seams, occurs primarily in sucrosic dolomite units. On weathered surfaces, spaced cleavage seams stand 1–2 mm above the surrounding rock material (Fig. 3d). On fresh surfaces, and in thin section the spaced cleavage appears as dark seams of clay (Fig. 6a). Dolomite in the microlithons is not as deformed as limestone layers above or below the dolomite (Fig. 4a). The spaced cleavage is sinuous; curvature is more marked in fold profile than on bedding surfaces. The penetrative cleavage and spaced cleavage are not parallel in most specimens, refraction occurs at lithologic boundaries (Fig. 4b).

STRAIN

Measurement of accumulated strain

Several members of the Conococheague Formation contain ooids that are used as accumulated strain markers. The orientation of maximum principal elongation and bulk finite strain axial ratio were measured in thin sections cut normal to the local fold axis. The long and short axes were digitized for 50 or more measurable ooids per thin section. Orientation of principal elongation and axial ratio, along with standard deviation of orientation and axial ratio were calculated for each thin section. Standard deviation of axial ratio and orientation decreases with the amount of strain, and is a function of the initial shape distribution of the particles being deformed (Cloos 1947, 1971; Ramsay 1967; Elliott 1970; Dunnet 1969). Accumulated strain data are presented in Table 1, along with cleavage orientations measured in thin section. Maximum elongation orientations fan around the fold hinge surface, as does cleavage. The amount of accumulated strain varies around folds; it is least on the shallowly dipping limbs of folds, intermediate on the steeply dipping limbs of folds, and greatest in the fold hinge zones (see Table 1).

Measurement of incremental strain

Preserved particle displacement paths in progressive deformation can be used to calculate the orientation and magnitude of the principal strain axes for each point on the displacement path (Durney & Ramsay 1973; Wickham 1973). When displacement paths are divided into a series of line chords of arbitrary length, the orientation of the principal strain axes can be calculated for each incremental line chord relative to an arbitrary, rotating reference frame assuming no area change (Durney & Ramsay 1973; Wickham 1973). Antitaxial fibrous growths of calcite on quartz grains in the Conococheague Formation preserve a displacement path for the sample in which they occur (Wickham 1973; Wickham & Anthony 1978). The strain tensor can be calculated for each strain increment (represented by a line chord on the fiber) and can be integrated to approximate finite strain.

Table 1. Mean and standard deviation of ooid long axis orientation, mean standard deviation of S_p orientation and location on the local fold. All measurements are in degrees relative to bedding. S_p was not well developed in sample 831. Sample 845 was a chert without measurable S_p. These data show the increase in strain from the shallowly dipping limbs of folds to the hinge zone

Sample	Mean axial ratio	Mean orientation of ooid long axis	Orientation standard deviation	Mean orientation of S_p	Standard deviation	Sample location
831	1.58	—	6.4	—	—	Shallow limb
938	1.9	57	6.1	52	5.9	Shallow limb
924	2.0	59	7.2	57	7.4	Shallow limb
928	2.1	44	8.4	44	5.9	Shallow limb
936	2.15	28	20.5	28.9	6.6	Shallow limb
930	2.6	76	7.3	77	3.9	Steep limb
845	3.1	—	16.3	—	—	Fold hinge

Fibers used in this study were not twinned or recrystallized. Only those fibers which grew from relatively isolated grains were used, minimizing the effect of interference of other grains on the motion of the particles. Equant or nearly equant grains were selected preferentially over inequant grains to limit the effect of grain shape on strain path.

Both fibers growing from isolated quartz grains, and fibers growing between quartz grains were used. The centroid of each grain was identified by measuring a series of grain diameters on photographic prints. Fibers were visually divided into equal length line segments, and the end points digitized. The data from each thin section are referred to a two-dimensional local orthogonal co-ordinate frame, where one axis is parallel with bedding in the fold profile.

The orientation of principal elongation, ellipse axial ratio and area strain were calculated for each increment from the displacement gradient matrix, and accumulated by matrix multiplication. The orientation of incremental and accumulated maximum principal elongation were determined for 119 data sets. Composite paths were prepared by accumulation of increments for all fiber sets in a sample. Fiber sets that displayed solution activity in their vicinity were not used in the preparation of the composite paths, because the calculations assume no volume change during deformation.

Four samples were suitable for the construction of composite strain paths (Fig. 2). The abscissa of each graph represents the angle of principal elongation to bedding, measured in a Lagrangian reference frame that is rotating passively during folding. The ordinate represents increasing time with $t = 0$ at the bottom. The location of each incremental strain path is shown on the fold profiles (Fig. 2).

Samples containing usable fibers were collected from both limbs of a fold; samples 850 and 939 (Fig. 2) are on the steep and shallow limbs of a fold, respectively. The strain path calculated for sample 850 shows an initial orientation of the principal shortening direction 30° to bedding. During folding, the incremental principal shortening axis rotated to a final orientation of 85°, almost perpendicular to bedding. This rotation is produced in part by the layer rigidly rotating during folding. The bed had an initial dip of 30° and a final dip of 85°, assuming that the local axis of principal shortening was horizontal. This final dip is in close agreement with the present day orientation of bedding (80° overturned). The initial orientation of the maximum principal shortening in sample 939 started 22° below bedding and rotated through the bedding to a final orientation of 43° (Fig. 2). The final orientation of maximum principal strain in sample 939 corresponds to a bedding dip of 43°E, assuming that the axis of maximum principal shortening was horizontal. The present dip of bedding in sample 939 is 45°E. The composite paths for samples 816 and 937, both from the shallow limbs of folds have the same general shape as sample 939 (Fig. 2). The change of principal directions from initial to final positions is dependent on its position on the fold. Samples from the steeply dipping limbs of folds show the greatest change of orientation, while samples from the hinge zones of folds show the smallest change in orientation.

Relationships of strain to folds

Deformation varies systematically around the folds, with the fold hinge accumulating the greatest strain, the steep limbs, intermediate strain and the shallow limbs the lowest strain. Incremental principal elongation orientations were initially oriented symmetrically about the hinge; however, marked asymmetry developed during folding. Straight or nearly-straight incremental elongation plots in the hinge zone show that deformation was nearly coaxial in the hinge zone, and that the hinge zones of folds did not migrate laterally. With layering inclined to compression, the steep limbs of the folds rotated the largest amount, while the shallow limbs rotated the least. Both limbs of folds exhibit markedly non-coaxial strain.

FABRIC ANALYSIS

Textures contributing to rock cleavage in the Conococheague were studied in thin section, by Field Emission Scanning Electron Microscope and X-ray diffraction. Crystal morphology and orientation were described in photographs from both optical and electron microscopy. Crystallographic orientation was determined by X-ray analysis of samples both normal to hinge lines and parallel to cleavages using a RIGAKU Semi-automated Pole Figure goniometer. Plots of reflected intensities were prepared for calcite $\{10\bar{1}1\}$ (*r* twin plane) and $\{11\bar{2}0\}$ (*a* axis), and for dolomite $\{10\bar{1}1\}$ (*r* twin plane); (notations are Bravais indicies). The samples are from various regions of folds.

Penetrative cleavage (S_p)

The penetrative cleavage (Fig. 5a) is formed by an interlocking mosaic of crystals (anastomosing texture of Borradaile *et al.* 1982), is not associated with alignment of platy particles such as randomly dispersed phyllosilicates, and is limited to the phyllosilicate-poor calcite microspar layers of the Conococheague Formation. The penetrative cleavage shows no evidence of neomorphism. The surfaces of dolomite grains in the microspar are serrated (Fig. 5b). Straight crystal boundaries are present in micrite (Fig. 5c), and both twinning and subgrain growth of calcite spar and microspar can be seen in ultra-thin, polished sections (Fig. 5c–e). Recrystallization textures seen are similar to those reported in some marbles (Vernon 1981) and include formation of subgrains along previous twins (Fig. 5d), and along grain boundaries (Fig. 5e).

The orientation of the penetrative cleavage varies throughout any one specimen, and its expression improves with increased strain (Cloos 1971). Fifty or more orientations of penetrative cleavage were measured in nine thin sections, four of which contained

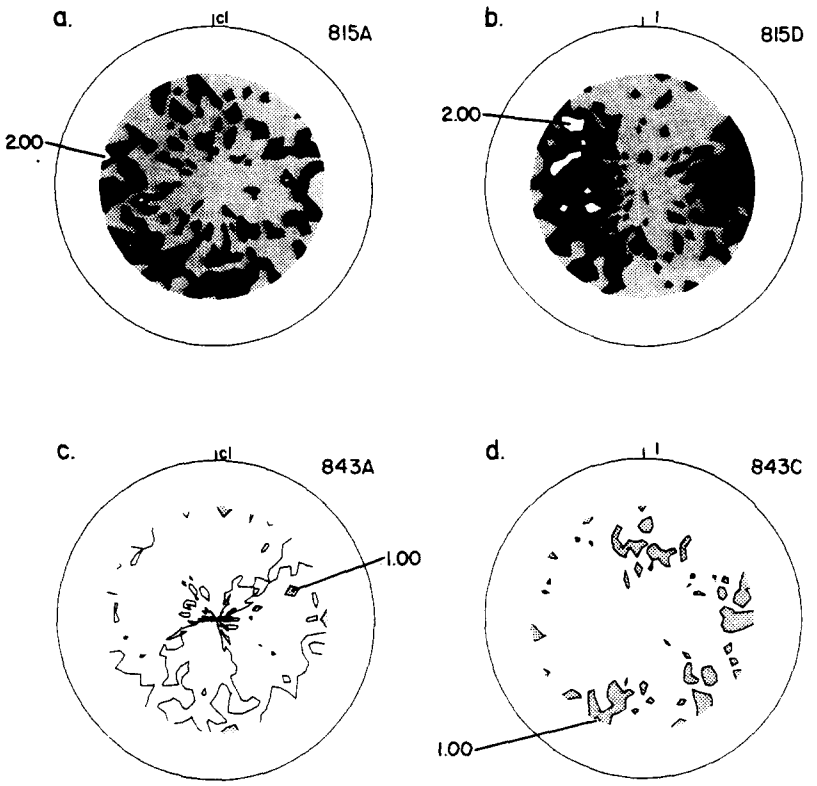

Fig. 7. Uninterpreted reflectance patterns for CuKa1 radiation for calcite $\{10\bar{1}1\}$ (notation is Bravais indices). Contour interval is 0.25. Values between 0.5 and 1.0 of mean random distribution (mdr) are shaded gray, values between 1.0 and 1.5 mdr are black, and values above 1.5 mdr are white. Maximum values are shown on individual patterns. These data were collected using a RIGAKU Semi-Automatic Pole Figure Goniometer. For calcite $\{10\bar{1}1\}$ the counter angle is 29.42 $2\theta/\theta$. The scans were run on a 5° spacing for Beta rotation and Alpha rotation. Beta scans from 0 to 360° were run for each 5° Alpha step. Background data were collected for each peak. Solnhofen limestone cut obliquely to bedding was used as a uniform standard for calcite. (a) Calcite $\{10\bar{1}1\}$ data for sample 815 cut perpendicular to hinge line of local fold. The cleavage trace is marked. (b) Calcite $\{10\bar{1}1\}$ data for sample 815 cut parallel with cleavage. The elongation direction is vertical. (c) Calcite $\{10\bar{1}1\}$ data for sample 843 cut perpendicular to hinge line of the local fold. The cleavage trace is vertical in the plot. (d) Calcite $\{10\bar{1}1\}$ data for sample 843 cut parallel with cleavage. The elongation direction is vertical.

deformed ooids (Table 1). There is good correlation between penetrative cleavage orientation and accumulated elongation orientation. Penetrative cleavage changes orientation in the vicinity of large dolomite grains. The cleavage trace is continuous, but refracted, as much as 14° at lithologic boundaries between limestone and dolomite layers, where penetrative cleavage changes to spaced cleavage.

Deformation of calcite

The truncation of large grains in the micritic matrix, along with the presence of unrotated phyllosilicates indicate that pervasive pressure solution was active for at least part of the deformation. The interlocking fabric, existence of twin planes, and formation of subgrains along twin planes show that ductile flattening followed by recrystallization is partly responsible for the deformation of limestones at low temperatures (lowest greenschist, and possibly metagenesis).

Deformation by twin gliding occurs at low temperatures and confining pressures, and samples show twinning in sparry calcite cement and microspar. Experimental work on deformation mechanisms in fine-grained carbonates has not produced pervasive pressure solution or recrystallization at temperatures below 400°C. The occurrence of recrystallization textures in low-grade metamorphic conditions implies that either strain rate or strain energy density may be more important than previously thought. Wenk *et al.* (1973) reported that at low temperatures (below 350°C), the plastic elongation of fine-grained samples does not develop appreciably after strains of 22%, and that recognizable recrystallization fabrics do not form below 500°C. The presence of recrystallization fabrics in the materials studied can be attributed to either a stronger dependence on strain rate than anticipated, or a threshold of strain energy density which, at temperatures within the metagenic range, would trigger recrystallization.

Uninterpreted X-ray reflectance patterns for limestone samples are shown in Fig. 7. (Note: only *r* twin plane $\{10\bar{1}1\}$ data are shown). Calcite from the shallowly dipping limb of a fold shows some organization of $\{10\bar{1}1\}$ along cleavage in fold profile, and along lineation on the cleavage surface (Fig. 7a & b; sample 815). These patterns show definite symmetry of $\{10\bar{1}1\}$ around lineation on the cleavage surface, (815D). There is only minor symmetry in the sample normal to the fold hinge line on the shallow limb, (815A). Organization of $\{10\bar{1}1\}$ is also seen in the hinge zone on both the fold normal plane,

(843A), and the cleavage plane, (843C) (Figs. 7c & d). These patterns show the formation of local maxima. The pattern in the hinge zone may show the formation of maxima about the elongation direction as is seen in experimentally deformed samples (cf. Wagner *et al.* 1982), but the data are not conclusive. No interpretation of which calcite twin or slip systems activated, or of the importance of recrystallization can be made from the X-ray data; however, the data do indicate that the amount of crystallographic orientation changes from limb to hinge, where strain rates where higher.

At low strain rates, and relatively low temperatures, the fine-grained limestones studied deform by a combination of pervasive pressure solution (Coble creep), twinning and recrystallization. Direct evidence of deformation by pervasive pressure solution is seen in the truncation of rigid grains. The degree of lattice preferred orientation in the micrite is less than in experimental samples that deformed by twinning and slip alone for similar values of shortening. Deformation by pervasive pressure solution can produce an elongate microfabric similar to that produced by twin gliding and slip. Both pervasive pressure solution, and twinning and slip can be activated during a single deformation, with the predominant mechanism depending on local strains and strain rates (strain energy density).

Spaced cleavage (S_s)

The spaced cleavage consists of zones or bands of phyllosilicates (Fig. 6a; rough cleavage of Borradaile *et al.* 1982), or continuous stringers of phyllosilicates (Fig. 6b; sinuous cleavage). Spaced cleavage is found in phyllosilicate-bearing dolomite layers (approximately 1% clay by volume), and in some cases extends into limestones at lithologic boundaries where it meets the penetrative cleavage. Spaced cleavage is not associated with the morphologic orientation of dolomite crystals, but truncates particles along its trace. The spaced cleavage connects with fibrous calcite and quartz fill in syntectonic tension gashes, and is present along boundaries of deformed ooids and quartz grains with calcite fibers.

The spaced cleavage is associated with the accumulation of insoluble minerals. Qualitative estimates of percentages of Al, Mg, Si, K and Ca across solution surfaces in six samples were made using an energy dispersive analyzer on the electron microprobe. Results show that these surfaces are enriched in Al, Mg, Si and K and are depleted in Ca relative to the intact rock. Data were also collected for Ti and Fe, but results were inconclusive. The elemental composition of the surface materials was verified using standard microprobe wavelength techniques with a 20 μm beam. Concentrations of elements in the microlithon and along the spaced cleavage surface were estimated by counting density of elemental excitation sites in 100 μm diameter circles, and are presented in Table 2. These abundances are only estimates, as one excitation site may not represent the same elemental concentration across the sample because of matrix effects.

The orientation of the spaced cleavage changes systematically across samples, forming curved cleavage surfaces. The change in orientation in dolomite layers, when measured from the center of a layer, is similar to the change of incremental principal directions as measured by the calcite fibers in nearby limestone layers (Table 3). The change in orientation of the spaced cleavage is greatest on the steeply dipping limb of the folds, and least in the hinge zone of the folds, as is the change of the incremental principal strain orientations. Measured orientations of the spaced cleavage (starting at the center and progressing toward the layer boundary) indicate that the spaced cleavage initiates at a point near the center of layering and propagates away from that point as deformation progresses. In samples 816 and 937 (Table 3), the initial and final orientation of the zones are remarkably close to the initial and final orientation of the incremental elongation axis.

The spacing between these cleavage surfaces also changes systematically with location in the fold (Table 4). These values were derived by counting the number of macroscopic spaced cleavages on traverses perpendicular to the spaced cleavage trace. In the hinge zones of folds, the spacing of these cleavage surfaces is less than

Table 2. Counts of excitation sites in matrix (microlithon) and along spaced cleavage zones from EDS electron dot maps. The maps were prepared using 60 s count times at each location. The values presented are averages from four counts of 100 micron diameter (scaled to sample) circles selected at random on the dot maps. The data show accumulation of Al, Mg, Si, K and depletion of Ca along the spaced cleavage

Sample	Beam location	Al	Mg	Si	K	Ca	Sample location
816	Matrix	14	22	13	14	96	Shallow limb
816	Cleavage zone	33	27	43	29	13	
937	Matrix	13	18	18	16	88	Shallow limb
937	Cleavage zone	22	28	30	19	8	
809	Matrix	5	5	19	14	110	Steep limb
809	Cleavage zone	14	8	28	21	21	
808	Matrix	11	8	16	9	106	Hinge zone
808	Cleavage zone	27	19	30	11	7	
811	Matrix	10	3	12	15	98	Hinge zone
811	Cleavage zone	28	7	43	24	10	
814	Matrix	14	23	12	24	120	Hinge zone
814	Cleavage zone	39	46	29	51	9	

Table 3. Initial and final orientations of incremental and accumulated strain and S_s. All measurements are relative to bedding and are in degrees. Samples 814 and 808 did not have incremental strain markers, but are included to show the low range in orientation of S_s in the hinge zones of folds

Sample	Initial incremental elongation axis orientation	Final incremental elongation axis orientation	Final accumulated elongation axis orientation	Initial S_s orientation	Final S_s orientation	Location on fold
816	110	62	80	112	65	Shallow limb
				101	54	
850	30	86	58			Steep limb
937	110	32	60	31	82	Shallow limb
939	112	46	68			Steep limb
814				101	91	Hinge zone
				116	93	
				110	100	
808				52	70	Hinge zone
				49	47	
				46	62	

4.8 mm. Spacing is 13 mm on the shallow limb in sample 816, and is between 5.7 and 8.5 mm on the steep limb. These data also indicate that the strain is greatest in the fold hinge zones and least on the shallowly dipping limbs of the folds.

Deformation of dolomite

The mechanisms of dolomite deformation are not as well understood as those of calcite (Wenk & Shore 1975), but experimental work has shown that the expected mechanisms in fine-grained dolomites below temperatures of 700°C should be predominantly slip and twinning. The dolomites examined in this study show a range of deformation mechanisms, depending on fold location and nature of grain contacts. Deformation on the limbs of folds is primarily by pressure solution, concentrating insoluble materials, and forming spaced cleavage. Textures attributed to ductile flattening by twinning, and recovery/recrystallization (subgrain growth) are observed in the hinge zones of folds, as well as textures attributed to pressure solution (Figs. 6c, d, e & f). Figure 6(c) shows an SEM image of a dolomite field from the hinge zone of a fold. The dolomite crystals are twinned, and a subgrain of dolomite is growing at a grain-grain contact. The new growth is devoid of fluid inclusions. We interpret this as evidence of strain-free subgrain growth. Fluid inclusions are common in the dolomites, and if recrystallization has occurred, fluid inclusions would be eliminated as new crystal boundaries sweep through the deformed crystal. The formation of subgrains in dolomites has not been examined experimentally, and the controlling factors are poorly understood. Figure 6(d) shows an ultra-thin polished section of a dolomite from the shallowly dipping limb of a fold and demonstrates twinning of dolomite grains in a calcite matrix. Figure 6(e) shows dolomite in the hinge zone of a fold where the individual dolomite crystals have serrated boundaries, and show subgrain growth. Figure 6(f) shows dolomite from a second fold hinge where pressure solution textures and subgrain growth can be seen.

Table 4. Spacing of solution zones in eight samples from various portions of folds. Spacing was measured perpendicular to the solution zone trace. Measurements are in cm

Location	Sample	Spacing (cm)	Material
Hinge	811	0.42	Dolomite
	814	0.48	Dolomite
	842	0.35	Limestone
	911	0.48	Dolomite
Steep limb	808	0.57	Dolomite
	809	0.85	Dolomite
	829	0.64	Limestone
Shallow limb	816	1.27	Dolomite

Dolomite does not show dimensional elongation or morphologic preferred orientation even though they are commonly twinned. If dolomite crystals occur in a calcite matrix, they are truncated by pressure solution at grain boundaries, and are twinned and fractured. Dolomite crystals in a predominantly dolomite matrix are twinned, and show subgrain growth in regions of high strain (Fig. 6c, e & f).

Uninterpreted reflectance patterns for dolomite samples are shown in Fig. 8. (Note: only *r* twin plane $\{10\bar{1}1\}$ data are shown.) Pole figure patterns for dolomites change with position on folds. On the shallowly dipping limb, the dolomites show only a minor amount of organization of $\{10\bar{1}1\}$ above random on the surface cut normal to the fold hinge line (Fig. 8a; sample 813); the pattern is slightly elongated perpendicular to the cleavage trace. Organization of $\{10\bar{1}1\}$ on the steep limb is slightly greater (Fig. 8 b & c; sample 912), with the migration of higher values toward the edge of the pattern and a minor symmetry of highs about the cleavage trace in 912A and the elongation direction in 912B. Organization of $\{10\bar{1}1\}$ in the hinge zone is greatest, showing distinct symmetry about the cleavage trace in 911A' and the lineation in 911B (Fig. 8d & e). The pole figure patterns are not directly comparable with published data on dolomites, but display a symmetric migration of reflected highs about the cleavage and lineation orientations seen in other naturally deformed dolomites (cf. Wenk & Shore 1975 for *c* axis data).

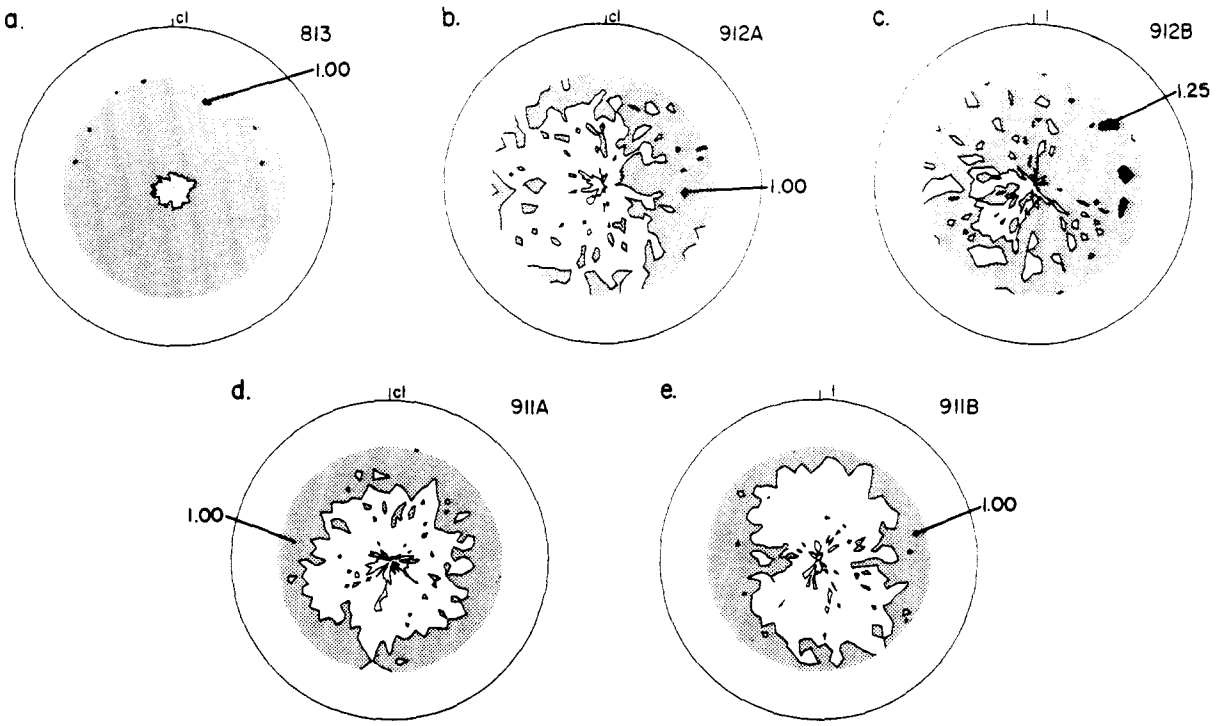

Fig. 8. Uninterpreted reflectance patterns for CuKa1 radiation for dolomite $\{10\bar{1}1\}$ (notation is Bravais indices). Contour interval is .25, maxima are noted on the plots. The angle for dolomite $\{10\bar{1}1\}$ is 30.94° $2\theta/\theta$. The scans were run using the same techniques as calcite. An unknown dolomite that displayed no preferred orientation was used for a uniform standard. (a) Dolomite $\{10\bar{1}1\}$ data for sample 813 cut perpendicular to the hinge line of the local fold. The cleavage trace is vertical. (b) Dolomite $\{10\bar{1}1\}$ data for sample 912 cut perpendicular to cleavage. The cleavage trace is vertical. (c) Dolomite $\{10\bar{1}1\}$ data for sample 912 cut parallel with cleavage. The elongation direction is vertical. (d) Dolomite $\{10\bar{1}1\}$ data for sample 911 cut perpendicular to local fold hinge line. The cleavage trace is vertical. (e) Dolomite $\{10\bar{1}1\}$ data for sample 911 cut parallel with cleavage. The elongation direction is vertical.

The truncation of material particles along the spaced cleavage zones, accumulation of insoluble materials, and the similarity of the orientation of the spaced cleavage surfaces to initial and final orientations of incremental elongation indicate that the spaced cleavage formed primarily due to pressure solution. However, dolomites between the solution surfaces display textures that indicate pressure solution, ductile flattening by twinning and possible grain boundary migration, and display recovery/recrystallization textures. The pole figure patterns for the dolomite samples show an increase in preferred orientation of the *r* twin plane $\{10\bar{1}1\}$ with the intensity and symmetry of the preferred orientation increasing with increased strain. Patterns in the fold hinge show the greatest alignment, and solution surfaces are closest in the fold hinges; twinning and recovery fabrics are also present in the fold hinges. We interpret the data to show that the deformation mechanisms for dolomite strongly depend on strain energy density, shifting from primarily pressure solution in low strain (and strain rate) conditions on the shallowly dipping hinges of folds to ductile mechanisms with recovery/recrystallization in higher strain (and strain rate) conditions in fold hinges. No interpretation of which slip or twin systems were activated or the importance of recrystallization in the formation of the fabrics preserved in the dolomites can be made from the data. However, our data indicate that strain rate and strain energy density may be more important in the behavior of dolomites than previously thought, and that incipient recovery/recrystallization can occur at relatively low temperatures in naturally deformed dolomites.

CONCLUSIONS

The Conococheague Formation contains two distinct syntectonic cleavage fabrics. A penetrative cleavage (S_p) formed in clean limestone layers, and a spaced cleavage (S_s) formed in sucrosic dolomite layers containing phyllosilicates. Both cleavage morphologies formed during a single, non-coaxial deformation event. Carbonate rocks examined in this study give an example of the behavior of calcite and dolomite during a natural, non-coaxial progressive deformation. The following interpretations are made from observations of the cleavage fabrics present in the Conococheague Formation in a portion of the Virginia Great Valley.

(1) Incremental strain markers show that layering was not initially parallel to the principal incremental shortening direction. The angle of inclination may have been as much as 30°. This resulted in the formation of asymmetric folds with cleavage fanning about the hinge surface of the folds. There is no evidence to indicate whether the units were tilted relative to the horizontal or whether the principal incremental shortening direction was tilted relative to horizontal layering.

(2) Fold hinges underwent coaxial deformation dur-

ing the folding process. Dolomite layers buckled during folding while interlayered limestones experienced at least some layer parallel shear. Deformation mechanisms of both limestone and dolomite seems to depend on strain rate and strain energy density. At lower strain rates, involving pressure solution and Coble creep, the rheology was probably Newtonian. At higher strain rates, in fold hinges, plastic mechanisms dominated, and stress–strain rate relationships apparently followed a power-law rheology.

(3) Cleavage in dolomites is preserved as spaced cleavage zones with insoluble materials, such as phyllosilicates, accumulated along them. The primary deformation mechanism in dolomites is pressure solution; however, twinning and recrystallization are important in highly strained fold hinge zones. At low strains, on the shallowly dipping limbs of folds, dolomite deformed by pressure solution, and the spacing of solution zones is large; twinning occurred in larger crystals. In regions of greater strain, the spacing of the solution surfaces is closer, and the importance of twinning (and possibly glide) increases, resulting in the formation of a minor crystallographic preferred orientation of dolomite. In the hinge zones of the folds, where the deformation is the greatest, the spacing of the solution surfaces is the closest, and the crystallographic orientation the greatest. Incipient recrystallization of dolomite also occurred in the fold hinge zones.

(4) Calcite deformed by pervasive pressure solution (Coble creep) and plastic flattening in the more intensely deformed samples. Pressure solution textures are present in the micrites but may not be preserved when insoluble materials are not present. Calcite also shows a change in deformation mechanism relative to fold location and strain rate. The progression of textures and deformation mechanisms are similar in dolomite and calcite. Fine-grained calcite apparently deforms by pervasive pressure solution (Coble creep) at low strain rates, with the deformation mechanism shifting to intracrystalline plastic mechanisms with higher values of strain (and strain rate) in the fold hinges.

(5) The spacing of pressure solution surfaces depends on the strain rate, and therefore strain energy density which varies with location on folds and lithology. Spacing of pressure solution cleavage is smallest in the hinge zone of folds and largest in the shallowly dipping limbs of folds. Spaced solution surface zones are curved, and have initial and final orientations similar to the observed incremental elongation which suggests that pressure solution zones originate at a point and propagate away, curving as the stress field changes orientation relative to bedding.

(6) We interpret the deformation of interbedded limestone and dolomite as follows. In the early stages of deformation, pervasive pressure solution (Coble creep) occurred in limestone, and widely spaced pressure solution zones occurred in dolomite layers. As the deformation progressed, strain energy increased in the hinge zones to the point that twinning and slip mechanisms became important in the limestones, while pressure solution was still dominant in the dolomites. With increased folding, limestone layers in hinge zones began to undergo syntectonic recovery and recrystallization. In the hinge zones of the folds, where strain energy is the greatest, dolomites began to deform by twinning and slip together with recovery or recrystallization. Changes in deformation mechanism from pressure solution to twinning and glide may localize fold hinge zones by changing the rheologic response of the hinge zone, from Newtonian viscous to power-law stress–strain rate relationships.

Acknowledgements—Funding for this study was provided by National Science Foundation grant EAR78-09248 to Wickham, and by the Geological Society of America in the form of Penrose Field grant No. 2400-78 to Tapp. Use of the electron microprobe at Phillips Petroleum Research Facility and the electron microanalyzer at the Oral Roberts University Department of Anatomy are gratefully acknowledged. Comments by Richard Groshong and an anonymous reviewer helped improve the manuscript. This paper represents a portion of Tapp's doctoral dissertation at the University of Oklahoma.

REFERENCES

Alterman, I. B. 1973. Rotation and dewatering during slaty cleavage formation: some new evidence and interpretations. *Geology* **1**, 33–36.

Alvarez, W., Engelder, T. & Geiser, P. A. 1978. Classification of solution cleavage in pelagic sediments. *Geology* **6**, 263–266.

Beutner, E. C. 1978. Slaty cleavage and related strain in Martinsburg slate, Delaware Water Gap, New Jersey. *Am. J. Sci.* **278**, 1–23.

Beutner, E. C. 1980. Slaty cleavage unrelated to tectonic dewatering: The Siamo and Michigamme slates revisited. *Bull. geol. Soc. Am.* **91**, 171–178.

Borradaile, G. J., Bayly, M. B. & Powell, C. McA. 1982 *Atlas of Deformational and Metamorphic Rock Fabrics*. Springer Verlag, New York.

Boulter, C. A. 1974. Tectonic deformation of soft sedimentary clastic dikes from the Precambrian rocks of Tasmania, Australia, with particular reference to their relations with cleavages. *Bull. geol. Soc. Am.* **81**, 589–609.

Butts, C. 1973 (reprint of 1940 Volume). *Geology of the Appalachian Valley in Virginia. Part 1—Geologic Text and Illustrations.* **52**, Virginia Division of Mineral Resources, Charlottesville, Virginia.

Clark, B. R. 1974. Mechanical formation of preferred orientation in clays. *Am. J. Sci.* **269**, 250–266.

Cloos, E. 1947. Oolite deformation in the South Mountain fold, Maryland. *Bull. geol. Soc. Am.* **58**, 843–918.

Cloos, E. 1971. *Microtectonics along the Western Edge of the Blue Ridge, Maryland and Virginia*. Johns Hopkins Press, Baltimore, Studies in Geology No. 20.

De Boer, R. B. 1977. On the thermodynamics of pressure solution Interaction between chemical and mechanical forces. *Geochim. cosmochim. Acta* **41**, 249–256.

De Sitter, L. U. 1964. *Structural Geology* (2nd edition). McGraw-Hill, New York.

Dietrich, D. & Song, H. 1984. Calcite fabrics in a natural shear environment, the Helvetic nappes of western Switzerland. *J. Struct. Geol.* **6**, 19–32.

Durney, D. W. 1972. Solution transfer, an important geological deformation mechanism. *Nature, Lond.* **235**, 315–317.

Durney, D. W. 1976. Pressure-solution and crystallization deformation. *Phil. Trans. R. Soc. Lond.* **A283**, 229–240.

Durney, D. W. 1978. Early theories and hypotheses on pressure-solution-redeposition. *Geology* **6**, 369–372.

Durney, D. W. & Ramsay, J. G. 1973. Incremental strains measured by syntectonic crystal growths. In: *Gravity and Tectonics* (edited by De Jong, K. A. and Scholten, R.). John Wiley, New York, 67–96.

Edmunson, R. S. & Nunn, W. E. 1973. Geology of the Berryville, Stephenson, and Boyce quadrangles, Virginia. Report of Investigations, **34**, Virginia Division of Mineral Resources, Charlottesville, Virginia.

Elliott, D. 1970. Determination of finite strain and initial shape from deformed elliptical objects. *Bull. geol. Soc. Am.* **81**, 2221–2236.

Elliott, D. 1973. Diffusion flow laws in metamorphic rocks. *Bull. Geol. Soc. Am.* **84**, 2645–2662.

Epstein, J. B. & Epstein, A. G. 1969. Geology of the Valley and Ridge Province between Delaware Water Gap and Lehigh Gap, Pennsylvania. In: *Geology of Selected Areas in New Jersey and Eastern Pennsylvania and Guidebook of Excursions* 1969 (edited by Subitzky S.). Annual Meeting, Geological Society of America, Atlantic City, New Jersey; New Brunswick Rutgers University Press, 132–205.

Fletcher, R. C. 1982. Coupling of diffusional mass transport and deformation in a tight rock. *Tectonophysics* **83**, 275–291.

Fletcher, R. C. & Pollard, D. D. 1981. Anticrack model for pressure solution surfaces. *Geology* **9**, 419–424.

Freeman, B. & Ferguson, C. C. 1986. Deformation mechanism maps and micromechanics of rocks with distributed grain sizes. *J. geophys. Res.* **91**, 3849–3860.

Geiser, P. A. 1974. Cleavage in some sedimentary rocks of the central Valley and Ridge Province, Maryland. *Bull. geol. Soc. Am.* **85**, 1399–1412.

Geiser, P. A. 1975. Slaty cleavage and the dewatering hypothesis, an examination of some critical evidence. *Geology* **3**, 717–720.

Gray, D. R. 1978. Cleavages in deformed psammitic rocks from south-eastern Australia: their nature and origin. *Bull. geol. Soc. Am.* **89**, 577–590.

Gray, D. R. 1981. Compound tectonic fabrics in singly folded rocks from southwest Virginia, U.S.A. *Tectonophysics* **78**, 229–248.

Groshong, R. H. 1975a. Strain, fractures, and pressure solution in natural single layer folds. *Bull. geol. Soc. Am.* **86**, 1363–1376.

Groshong, R. H., Jr. 1975b. "Slip" cleavage caused by pressure solution in a buckle fold. *Geology* **3**, 411–413.

Groshong, R. H., Jr. 1976. Strain and pressure solution in the Martinsburg slate, Delaware Water Gap, New Jersey. *Am. J. Sci.* **276**, 1131–1146.

Groshong, R. H., Pfiffner, O. A. & Pringle, L. R. 1984. Strain partitioning in the Helvetic thrust belt of eastern Switzerland from the leading edge to the internal zone. *J. Struct. Geol.* **6**, 5–18.

Heald, M. T. 1955, Stylolites in sandstones. *J. Geol.* **63**, 101–114.

Hobbs, B. E., Means, W. D. & Williams, P. F. 1976. *An Outline of Structural Geology*. John Wiley and Sons, New York.

Holeywell, R. C. & Tullis, T. E. 1975. Mineral reorientation and slaty cleavage in the Martinsburg Formation, Lehigh Gap, Pennsylvania. *Bull. geol. Soc. Am* **86**, 1296–1304.

Jeffery, G. B. 1923. The motion of ellipsoidal particles immersed in a viscous fluid. *Proc. R. Soc. Lond.* **102A**, 161–179.

Kamb, W. B. 1959. Theory of preferred orientations developed by crystallization under stress. *J. Geol.* **67**, 153–170.

Langdon, T. G. 1985. Regimes of plastic deformation. In: *Preferred Orientation in Deformed Metals and Rocks: An Introduction to Modern Textural Analysis* (edited by Wenk, H.-R.). Academic Press, New York, 219–232.

March, A. 1932. Mathematische Theorie der Regelung nach der Korngestalt bei ein affiner Deformation. *Z. Krystallogr.* **81**, 285–297.

Marshak, S. & Engelder, T. 1985. Development of cleavage in limestones of a fold-thrust belt in eastern New York. *J. Struct. Geol.* **7**, 345–360.

Means, W. D. 1977. Experimental contributions to the study of foliations in rocks: a review of research since 1960. *Tectonophysics* **39**, 329–354.

Mercier, J.-C. C. 1985, Olivine and pyroxenes. In: *Preferred Orientation in Deformed Metals and Rocks: An Introduction to Modern Textural Analysis* (edited by Wenk, H.-R.). Academic Press, New York, 407–430.

Maxwell, J. C. 1962. Origin of slaty and fracture cleavage in the Delaware Water Gap area, New Jersey and Pennsylvania. *Geol. Soc. Am.*, Buddington Volume, 281–311.

Patalakha, E. I. & Polyakov, A. I. 1977. The thermal effects of tectonic deformations. *Geologiya Geophyz.* **18**, 14–22.

Plessman, von W. 1964. Gesteinlosung, ein Hauptfactor bein Schieferungsprozess. *Geol. Mitteilungen* **4**, 69–82.

Plessman, von W. 1966. Solution, deformation, transportation and structure (in German). *Z. Dt. geol. Ges.* **115**, 650–663.

Powell, C. McA. 1974. Timing of slaty cleavage during folding of Precambrian rocks, Northwest Tasmania. *Bull. geol. Soc. Am.* **85**, 1043–1060.

Price, G. P. 1985. Preferred orientations in quartzites. In: *Preferred Orientation in Deformed Metals and Rocks: An Introduction to Modern Textural Analysis* (edited by Wenk, H.-R.). Academic Press, New York, 385–407.

Ramsay, J. G. 1967. *Folding and Fracturing of Rocks*. McGraw-Hill, New York.

Roy, A. B. 1978. Evolution of slaty cleavage in relation to diagenesis and metamorphism: A study from the Hunsruckschiefer. *Bull. geol. Soc. Am.* **89**, 1775–1785.

Rutter, E. H. 1974. The influence of temperature, strain rate and interstitial water in the experimental deformation of calcite rocks. *Tectonophysics* **22**, 311–334.

Rutter, E. H. 1976. The kinetics of rock deformation by pressure solution. *Phil. Trans. R. Soc. Lond.* **A283**, 203–219.

Rutter, E. H. & Rusbridge, M. 1977. The effect of non-coaxial strain paths on crystallographic preferred orientation development in the experimental deformation of a marble. *Tectonophysics* **39**, 73–86.

Siddans, A. W. B. 1972. Slaty cleavage—a review of research done since 1815. *Earth Sci. Rev.* **8**, 205–232.

Sorby, H. C. 1853. On the origin of slaty cleavage. *Edinburgh New Phil. J.* **55**, 137–148.

Sprunt, E. S. & Nur, A. 1977. Destruction of porosity through pressure solution. *Geophysics* **42**, 726–741.

Spry, A. 1968. *Metamorphic Textures*. Pergamon Press, Oxford.

Tullis, T. E. 1976. Experiments on the origin of slaty cleavage and schistosity. *Bull. geol. Soc. Am.* **87**, 745–753.

Wagner, F., Wenk, H. -R., Kern, H., Van Houtte, P. & Esling, C. 1982. Development of preferred orientation in plane strain deformed limestone: experiment and theory. *Contr. Miner. Petrol.* **80**, 123–139.

Watson, G. S. 1970. Orientation statistics in the earth sciences. *Bull. geol. Instn Univ. Uppsala*, New Series **2**, 73–89.

Wenk, H.-R. 1985. Carbonates. In: *Preferred Orientation in Deformed Metals and Rocks: An Introduction to Modern Textural Analysis* (edited by Wenk, H.-R.). Academic Press, New York, 361–384.

Wenk, H. -R., Kern, H. & Wagner, F. 1981. Texture development in experimentally deformed limestone. Deformation of Polycrystals: mechanisms and microstructures. *Proc. 2nd Risø Int. Symp. Metall. Mater. Sci.* 235–245.

Wenk, H. -R. & Shore, J. 1975. Preferred orientation in experimentally deformed dolomite. *Contr. Miner. Petrol.* **50**, 115–126.

Wenk, H.-R., Takeshita, T., Van Houtte, P. & Wagner, F. 1986. Plastic anisotropy and texture development in calcite polycrystals. *J. geophys. Res.* **91**, 3861–3869.

Wenk, H. -R., Venkitasubramanyan, C. S., Baker, D. W. & Turner, F. J. 1973. Preferred orientation in experimentally deformed limestone. *Contr. Miner. Petrol.* **38**, 81–114.

Weyl, P. K. 1959. Pressure solution and the force of crystallization a phenomenological theory. *J. geophys. Res.* **64**, 2001–2025.

Wickham, J. S. 1972. Structural geology of a portion of the Blue Ridge, northern Virginia. *Bull. geol. Soc. Am.* **83**, 723–760.

Wickham, J. S. 1973. An estimate of strain increments in a naturally deformed carbonate rock. *Am. J. Sci.* **273**, 23–47.

Wickham, J. S. & Anthony, M. 1978. Strain paths and folding of carbonate rocks near Blue Ridge, central Appalachians. *Bull. geol. Soc. Am.* **88**, 920–924.

Williams, P. F., Collins, A. R. & Wiltshire, R. G. 1969. Cleavage and penecontemporaneous deformation structures in sedimentary rocks. *J. Geol.* **77**, 415–425.

Willis, D. G. 1977. A kinematic model of preferred orientation. *Bull. geol. Soc. Am.* **88**, 883–894.

Wood, D. S. 1974. Current views of the development of slaty cleavage. *Annu. Rev. Earth Planet. Sci.* **2**, 369–401.

Vernon, R. H. 1981. Optical microstructure of partly recrystallized calcite in some naturally deformed marbles. *Tectonophysics* **78**, 601–612.